Dynamic Article Links ►

Cite this: DOI: 10.1039/c0xx00000x

www.rsc.org/xxxxxx

ARTICLE TYPE

Cyanide-Bridged Bimetallic 3D Hoffman-Like Coordination Polymers with Tunable Magnetic Behaviour

Jin-Yan Li, Zhao-Ping Ni, Zheng Yan, Ze-Min Zhang, Yan-Cong Chen, Wei Liu and Ming-Liang Tong*

Received (in XXX, XXX) XthXXXXXXXXX 20XX, Accepted Xth XXXXXXXXX 20XX

DOI: 10.1039/b000000x

Three cyanide-bridged bimetallic coordination polymers $[Fe(bpmp)\{Ag(CN)_2\}_2]\cdot 0.5DMF\cdot 0.5EtOH\cdot 2H_2O$ (**1**), $[Fe(bpmp)\{Au(CN)_2\}_2]\cdot DMF\cdot 0.5EtOH\cdot H_2O$ (**2**) and $[Fe(bpmp)\{Ni(CN)_4\}]$ (**3**) (bpmp = 1,4-bis(pyridin-4-ylmethyl)piperazine), have been synthesized and characterized. Single crystal X-ray analysis shows that **1** and **2** are isostructural with 3D doubly interpenetrated Hoffman-like network without metallophilic interactions, while **3** shows 3D pronouncedly distorted Hoffman framework. Magnetic susceptibility measurements exhibit two-step spin transition properties in **1** and **2**, whereas a characteristic paramagnetic behaviour in **3**, respectively.

Introduction

Spin-crossover (SCO) complexes can exhibit magnetic responses to subtle external stimuli, e.g., temperature, light, pressure and guest molecules, involving simultaneously changes of colour, dielectric constant and electrical resistance.[1-6] Thus, these SCO materials provide potential applications in data storage and display devices.[1] Most such applications require an abrupt SCO with broad thermal hysteresis around room temperature.[7] To achieve this ultimate goal, many research workers have investigated the SCO properties by adjusting the nature of ligands, uncoordinating counterions and solvent molecules.[8]

Among the SCO families, six-coordinated iron(II) SCO materials represent a typical and significant system, in which the d^6 electronic configuration may switch between paramagnetic high-spin (HS) state and diamagnetic low-spin (LS) state by external perturbations.[4,9] Among them, the Hoffman-like coordination polymers have been investigated for years.[9] They can be classified into two main series, that is, $[Fe(L)_n\{M^{II}(CN)_4\}]$ (L represents bis-monodentate or monodentate pyridine-like ligand, n = 1 or 2, M^{II} may be Ni, Pd or Pt)[10] and $[Fe(L)_n\{M^{I}(CN)_2\}]$ (L is the same as that mentioned above, n = 1 or 2, M^{I} may be Cu, Ag or Au).[11] These metallocyanate ligands are rigid enough, resulting in the strong cooperativity between SCO active centres. The pillared ligands can adjust both the SCO properties and porosity, making them appealing for potential chemical sensing applications.

Here, we chose the semi-rigid organic ligand 1,4-bis(pyridin-4-ylmethyl)piperazine (bpmp) as the pillared ligand, which offers two most stable chair and boat conformations.[12] Incorporating the bpmp ligand with iron(II) salts and cyano-metallate complexes, three Hoffman-like coordination polymers, $[Fe(bpmp)\{Ag(CN)_2\}_2]\cdot 0.5DMF\cdot 0.5EtOH\cdot 2H_2O$ (**1**), $[Fe(bpmp)\{Au(CN)_2\}_2]\cdot DMF\cdot 0.5EtOH\cdot H_2O$ (**2**) and $[Fe(bpmp)\{Ni(CN)_4\}]$ (**3**), were successfully obtained. Compounds **1** and **2** are essentially isostructural and undergo complete two-step spin transitions, while **3** displays paramagnetic behaviour.

Experimental

Materials and General Procedures

All of the reagents used in this work were got from commercial sources without further purification. Magnetic susceptibility measurements were performed on a Quantum Design MPMS instrument operating under a field of 1000 Oe. The diamagnetic correction for each sample was obtained from Pascal's constants. C, H, and N microanalyses were performed on fresh sample, with Elementar Vario-EL CHN elemental analyzer. FT-IR spectra were recorded in KBr tablets in the range of 4000-400 cm^{-1} with Bio-Rad FTS-7 spectrometer. Thermogravimetric (TG) analyses were carried out on NETZSCH TG209F3 thermogravimetric analyzer.

Synthesis

$[Fe(bpmp)\{Ag(CN)_2\}_2]\cdot 0.5DMF\cdot 0.5EtOH\cdot 2H_2O$ (**1**): This compound was synthesized by slow diffusion technique. A solution of $K[Ag(CN)_2]$ (20 mg, 0.010 mmol) and bpmp (14 mg, 0.05 mmol) in DMF was placed in a 5 mL test tube, whilst a 1 mL test tube was filled with a solution of $Fe(ClO_4)_2\cdot 9H_2O$ (21 mg, 0.05 mmol) in EtOH. The two vessels were then inserted into a40mL vial filled with EtOH. We collected yellow block crystals suitable for single crystal X-ray diffraction after two weeks. Yield: 75%. The amount of disordered solvent molecules in the crystal was determined by microanalysis and thermogravimetric analysis. Elemental analysis calcd (%) for$C_{22.5}H_{30.5}N_{8.5}O_3Ag_2Fe$: C 36.54, H 4.15, N 16.10; found: C 36.83, H 4.05, N 16.29. IR data for **1** (KBr, cm^{-1}): $\tilde{\nu}$ = 3400 (m), 3051 (m), 2936 (m), 2901 (m), 2819 (s), 2703 (w), 2162 (s), 2106 (m), 1656 (s), 1612 (s), 1561 (m), 1500 (m), 1425 (s), 1386 (s), 1250 (w), 1093 (s), 1011 (s), 930 (w), 839 (m), 802 (m), 781 (w).

[Fe(bpmp){Au(CN)$_2$}$_2$]·DMF·0.5EtOH·H_2O (**2**): The desired compound **2** was obtained as block yellow crystals using the procedure described above for **1**, excepting that the K[Au(CN)$_2$] was used in place of K[Ag(CN)$_2$]. Yield: 75%. The amount of disordered solvent molecules in the crystal was determined by microanalysis and thermogravimetric analysis. Elemental analysis calcd (%) for $C_{24}H_{32}N_9O_{2.5}Au_2Fe$: C 30.78, H 3.44, N 13.46; found: C 30.65, H 3.29, N 13.71. IR data for **2** (KBr, cm^{-1}): $\tilde{\nu}$ = 3411 (m), 3075 (m), 2939 (m), 2881 (m), 2809 (s), 2694 (w), 2171 (s), 1677 (s), 1610 (s), 1560 (m), 1498 (m), 1425 (s), 1388 (s), 1222 (w), 1090 (s), 1016 (s), 931 (w), 848 (m), 809 (m), 790 (w).

[Fe(bpmp){Ni(CN)$_4$}] (**3**): A solution of $FeSO_4 \cdot 7H_2O$ (0.028 g, 0.1 mmol), bpmp (0.028 g, 0.1 mmol) and K_2[Ni(CN)$_4$] (0.024 g, 0.1 mmol) in EtOH/H_2O (7 mL/3 mL) was sealed in a 15 mL Teflon-lined reactor and heated at 120 °C for 48 hours, then cooled to room temperature at the rate of 5 °C/h. Subsequently, square shaped yellow crystals suitable for single crystal X-ray diffraction were collected artificially. Yield: 40%; elemental analysis calcd (%) for $C_{20}H_{20}N_8FeNi$: C 49.33, H 4.14, N 23.01; found: C 48.99, H 4.12, N 22.83. IR data for **3** (KBr, cm^{-1}): $\tilde{\nu}$ = 3079 (m), 2942 (s), 2915 (m), 2879 (m), 2816 (s), 2140 (s), 1610 (s), 1562 (m), 1457 (s), 1427 (s), 1290 (s), 1226 (m), 1012 (s), 846 (s), 804 (s), 732 (w).

Table1 Crystal data of compounds **1-3**.

	1			**2**		**3**
T [K]	150(2)	225(2)	300(2)	100(2)	273(2)	150(2)
formula	$C_{22.5}H_{30.5}N_{8.5}O_3Ag_2Fe$	$C_{22.5}H_{30.5}N_{8.5}O_3Ag_2Fe$	$C_{22.5}H_{30.5}N_{8.5}O_3Ag_2Fe$	$C_{24}H_{32}N_9O_{2.5}Au_2Fe$	$C_{24}H_{32}N_9O_{2.5}Au_2Fe$	$C_{20}H_{20}N_8FeNi$
M_r	739.64	739.64	739.64	936.37	936.37	487.00
crystal system	monoclinic	monoclinic	monoclinic	monoclinic	monoclinic	monoclinic
space group	$C2/c$	$C2/c$	$C2/c$	$C2/c$	$C2/c$	$P2_1/c$
a [Å]	16.2400(7)	16.3171(9)	16.622(2)	16.4515(8)	16.7493(16)	11.5168(11)
b [Å]	13.6625(5)	13.8577(5)	13.9014(10)	14.2025(7)	14.8047(14)	10.1374(8)
c [Å]	14.8867(7)	14.8466(9)	15.434(3)	14.2637(7)	14.5137(12)	9.6121(9)
β [°]	111.728(5)	111.744(6)	112.586(17)	112.0840(10)	113.493(3)	103.266(3)
V [Å^3]	3068.4(2)	3118.2(3)	3292.7(7)	3088.2(3)	3300.6(5)	1092.27(17)
Z	4	4	4	4	4	2
D_c (mg cm^{-3})	1.601	1.576	1.492	2.014	1.884	1.481
F(000)	1476	1476	1476	1772	1772	500
crystal size (mm)	0.42×0.32×0.25	0.42×0.32×0.25	0.42×0.32×0.25	0.12×0.11×0.10	0.12×0.11×0.10	0.07×0.05×0.04
No. of total reflections	2307	2339	2463	3504	3742	2073
No. of reflections [$I > 2\sigma(I)$]	2099	2035	1877	2951	2424	1329
R_1 [$I > 2\sigma(I)$]	0.0448 (Squeeze)	0.0528 (Squeeze)	0.0682 (Squeeze)	0.0434 (Squeeze)	0.0660 (Squeeze)	0.0396
wR_2 [$I > 2\sigma(I)$]	0.1139 (Squeeze)	0.1419 (Squeeze)	0.1835 (Squeeze)	0.0971 (Squeeze)	0.1731 (Squeeze)	0.0846
S	1.125	1.095	1.145	1.102	1.125	0.982
CCDC number	987371	987372	987373	987374	987375	987376

X-ray Crystallography

Diffraction intensities of **1**were collected on an Oxford Diffraction Gemini R CCD diffractometer with Cu$_{K\alpha}$ radiation (λ = 1.54178 Å) at 150(2) K,225(2) K and 300(2) K, respectively.The intensity data of **2**and **3**were recorded on a Rigaku R-AXIS SPIDE IP system with MoK_α radiation, the crystal was cooled using a N_2 blower, OXFORD CRYOSYSTEMS-700 Series Cryostream Cooler. The structures were solved by direct methods, and all non-hydrogen atoms were refined anisotropically by least-squares on F^2 using the SHELXTL program. Hydrogen atoms on organic ligands were generated by the riding mode.[13] For **1** and **2**, the disordered DMF, ethanol and H_2O molecules could not be modelled properly; thus, the program SQUEEZE,[14] a part of the PLATON package of crystallographic software, was used to calculate the solvent disorder area and remove its contribution to the overall intensity data.

Results

Single Crystal X-ray Structures

The crystal structure determinations were performed at 300 K, 225 K and 150 K for **1** when performed at 273 K and 100 K for **2**. The structures of **1** and **2** are essentially the same. They crystallize in the monoclinic space group *C*2/*c* whatever the temperature is. Crystal and refinement data are displayed in Table 1, and the selected bond lengths and angles are given in Tables S1 and S2.

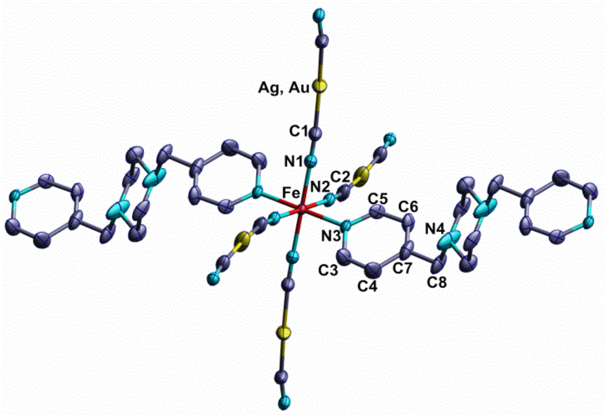

Fig. 1A representative fragment of **1** including the non-hydrogen atom numbering. The same atom numbering applies for compound **2** as they are isostructural to each other. Thermal ellipsoids are shown at 50% probability.

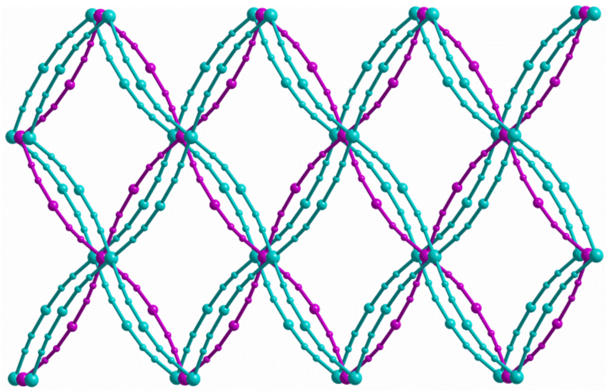

Fig. 2 View of the 2D $\{Fe[Ag(CN)_2]_2\}_\infty$ sheets formed by $\{Fe_4[M^I(CN)_2]_4\}$ grids. The same sheets are in one colour.

Since compound **1** and **2**are isostructural, the structure of **2** at 273 K will be described together with that of **1** at 300 K. All iron centres are equivalent and located on inversion centres in the structure. And the iron centre is situated in the middle of an octahedron defined by $[FeN_6]$ sphere. As shown in Fig. 1, the iron(II) coordination sphere consists of equatorial cyanide donor groups from four separate $[M^I(CN)_2]^-$ linkers and axial pyridyl donors belonging to two bpmp organic ligands. The piperazine ring of bpmp lies disordered about another inversion centre. And unique pyridin-4-yl ring is unequally disordered over two sites [site occupation values 0.513(13) and 0.487(13) for **1**, 0.529(15) and 0.471(15) for **2**]. Compared the axial Fe-N bond distances (Fe-N3) and the equatorial ones (Fe-N1, Fe-N2), we can note that the former are always larger than the latter, namely, Fe-N3 = 2.198(7) (2.178(10)) Å and Fe-N1 = 2.115(7) (2.111(9)) Å; Fe-N2 = 2.128(8) (2.123(9)) Å for **1** and **2** (in the parentheses), respectively. Considering the average Fe-N bond distances (<Fe-N> = 2.147(8) Å **1**; 2.137(10) Å **2**), both of them are fully high spin. As depicted in Fig. 2, the $[M^I(CN)_2]^-$ groups bridge iron centres to form extended 2D sheets with $\{Fe_4[M^I(CN)_2]_4\}$ grids. The $[Fe\text{-}NC\text{-}M^I\text{-}CN\text{-}Fe]_\infty$ chains in a 2D sheet are undulating as the angle C1-Ag-C2 of 173.9(5)°, Fe1-N1-C1 of 171.1(9)° and Fe1-N2-C2 of 169.1(8)° for **1** [C1-Au-C2 of 176.7(5)°, Fe1-N1-C1 of 174.4(12)° and Fe1-N2-C2 of 167.1(10)° for **2**], and two adjacent parallel chains show opposite shapes. Simultaneously, the bpmp ligands thread the meshes of the immediately adjacent sheets and ligate with iron atoms belonging to the subsequent 2D sheet, which confers two independent interpenetrated 3D networks (Fig. 3 and Fig. S1). The Fe···Fe distances through Fe-NC-M^I-CN-Fe edge are 10.3858(12) Å and 10.3661(7) Å for **1** and **2**, respectively, whereas the iron to iron distances along Fe-bpmp-Fe direction are 16.622(2) Å and 16.7493(16) Å for **1** and **2**, respectively. Unlike other $[M^I(CN)_2]^-$ (M = Ag and Au) bridged Hoffman-like systems,[9] no notable argentophilic or augentophilic interactions have been observed. And the framework can be simplified as a doubly interpenetrated 6-connected pcu net with the Schläfli symbol of $(4^{12}\cdot 6^3)$ (see Fig. S2).

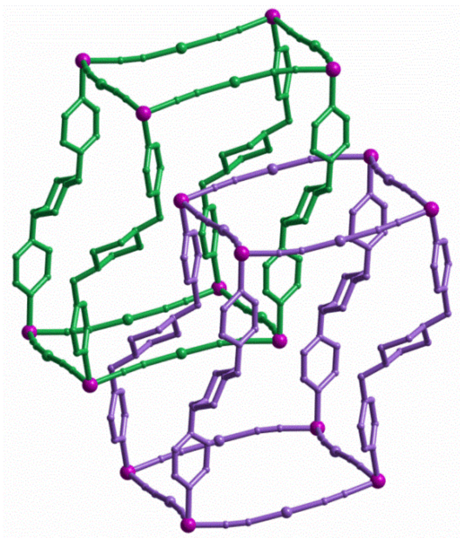

Fig. 3 View of two-fold interpenetrated frameworks of **1**. Fe: pink; net 1: green; net 2: purple.

Although the crystal structure of **1** at 150 K (**2** at 100 K) is the same as that at 300 K (**2** at 273 K), some obvious structural changes have been observed, especially for the FeN_6 octahedral coordination core. The average axial and equatorial Fe-N bond lengths decrease by 0.193(7) Å (0.173(10) Å **2**) and 0.193(8) Å (0.182(9) Å **2**), respectively. The total variations of 0.193(8) Å (**1**) and 0.179(10) Å (**2**) in the average Fe-N bond lengths clearly indicate the presence of HS↔LS spin transitions, which are also reflected in the changes of the unit-cell volumes (224.3 Å and 212.4 Å for compounds **1** and **2**, respectively). In addition, non-ignorable bond angle variations are also observed. That is, the variation of Fe1-N1-C1 is 4.9° (3.7° **2**), Fe1-N2-C2 is 5.9° (7.1°**2**), M^{I}-C1-N1 is 2.3° (2.7° **2**), M^{I}-C2-N2 is 4.2° (1.8° **2**).

The crystallographic analysis of **3** was performed at 150 K. It crystallized in the monoclinic $P2_1/c$ space group. The crystallographic data is shown in Table 1, and selected bond lengths and angles are given in Table S3. Considering the structure of **3**, the asymmetric unit contains half iron atom, which adopts a FeN_6 octahedral coordination geometry with the Fe-N average bond length of 2.18 Å. This magnitude of bond length is characteristic of iron(II) site in the HS state. As shown in Fig. 4, the equatorial positions of the FeN_6 octahedron are occupied by four N atoms belonging to four separate $[Ni(CN)_4]^{2-}$groups, which play the roles of linking four iron centres to form 2D layers of $[FeNi(CN)_4]_\infty$. While the bpmp organic ligands bridge axially the iron centres

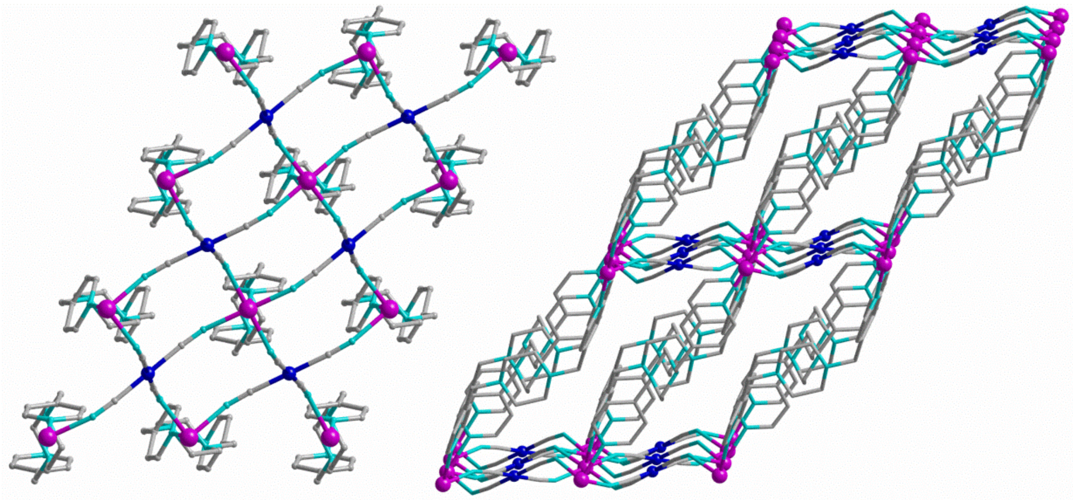

Fig.4A fragment of **3** shows the stacking layers of $[FeNi(CN)_4]_\infty$ (left); view of its 3D Hoffman-type framework (right).

leading to the anticipated 3D Hoffman-type framework. The Fe and Ni atoms in the structure are located on inversion centres. The piperazine ring of bpmp lies about another inversion centre, but no disorder is observed for piperazine or pyridin-4-yl rings when compared with that of compound **1** and **2**.

Magnetic Properties

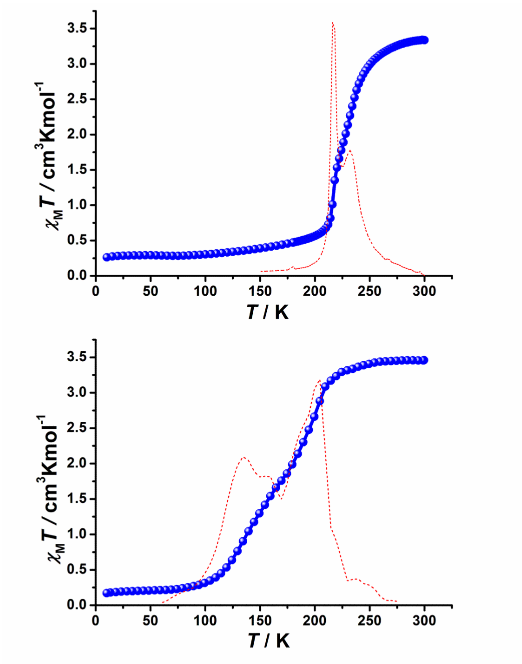

Fig. 5 Plots of $\chi_M T$ versus T (blue) and the corresponding derivative (red dot line) of **1** (above) and **2** (below).

The temperature dependence of the $\chi_M T$ plot for **1** is depicted in the Fig.5 (in which χ_M is the molar magnetic susceptibility and T is the temperature.). At 300 K, the value of $\chi_M T$ is equal to 3.34 cm^{3}Kmol^{-1} indicating the HS state for an iron(II) ion. The $\chi_M T$ remains constant upon cooling to 280 K. As the temperature is further lowered, it drops markedly witha two-step spin-transition, which is reflected in the derivative of the plot of $\chi_M T$ versus T. This SCO behaviour accomplishes at 150 K. Below this temperature, the $\chi_M T$ remains nearly constant with a value about 0.22~0.38 cm^{3}Kmol^{-1} suggesting the practically complete spin-transition. The critical temperatures are 232 K and 216 K, respectively. The warming process is nearly identical with the cooling one, that is, no hysteresis is observed.

The magnetic property of **2** is shown in Fig. 5. The $\chi_M T$ is 3.45 cm^{3}Kmol^{-1} at 300 K, which is in the range of the values expected for one HS iron(II) ion. Upon lowering the temperature, $\chi_M T$ remains constant down to 225 K and then decreases gradually, defining a complete two-step spin transition that ends at 75 K with critical temperatures of 204 K and 134 K, respectively. The steps are evidenced by the derivative of the plot of $\chi_M T$ versus T. Although we have also carried out the warming process for magnetic measurement, it is almost the same as the cooling one, indicating the absence of thermal hysteresis.

For the magnetic behaviour of **3**, in contrast to the Ag and Au derivatives, it is characteristic of the HS state (see Fig. S4). The value of $\chi_M T$ is equal to 3.40 cm^{3}Kmol^{-1} at 300 K, which is indicative of an iron(II) centre in the HS state. As the temperature is lowered, $\chi_M T$ remains approximately constant down to 50 K and then decreases rapidly due to the zero field splitting (ZFS) of the HS iron centres.

Discussion

Self-assembly of ternary system with Fe(II), $[M^I(CN)_2]^-/[M^{II}(CN)_4]^{2-}$ and bipyridine-like ligand has generated a variety of SCO-active coordination polymers.[10,11] Most of them were constructed into Hoffman-like networks. In this work, the syntheses and structural−magneto relationships of three Hoffman-like coordination polymers, $[Fe(bpmp)\{Ag(CN)_2\}_2]\cdot0.5DMF\cdot0.5EtOH\cdot2H_2O$ (**1**), $[Fe(bpmp)\{Au(CN)_2\}_2]\cdot DMF\cdot0.5EtOH\cdot H_2O$ (**2**) and $[Fe(bpmp)\{Ni(CN)_4\}]$ (**3**), were investigated. **1** and **2** are essentially isostructural to each other. Their framework structures can be viewed as 3D two-fold interpenetrated networks consisting of a stack of layers that made up of $[M^I(CN)_2]^-$ and Fe(II) defining the $\{Fe_4[M^I(CN)_2]_4\}$ grids. The closest double layers can be organized as one group. The bpmp lies in the axial position as the linker of layers. Thissemi-rigid organic ligand with stable chair conformation threads the grid of adjacent layer and connects with iron atom belonging to the subsequent layer, defining a3D interpenetrated architecture. Compared with most of the $[Fe(L)_2\{M^I(CN)_2\}]$ or $[Fe(L)\{M^I(CN)_2\}]$ systems, a significant difference emerges in the structures of compounds **1** and **2**: the metallophilic interactions are absent in our frameworks, which has been noted for a few examples, such as $\{Fe(5\text{-Br-}pmd)[Ag(CN)_2]_2\}$.[15] This distinction may arise from the undulating nature of the 2D sheets constituted by Fe(II) and $[M^I(CN)_2]^-$ groups, in which two adjacent parallel $[Fe\text{-}NC\text{-}M^I\text{-}CN\text{-}Fe]_\infty$ chains display opposite shapes. On closer inspection of the spin transition of both Ag and Au derivatives, we can note an obvious down−shift tendency of T_c when changing from Ag to Au. This tendency can be ascribed to the relativistic effects in heavy atoms. That is, Au exists the higher electron affinity when compared with Ag.[16] As a result, a stronger electron withdrawing effect on the CN group of $[M^I(CN)_2]^-$ would be observed for the Au derivative, then it should be expected poorer donor capacity for its N atoms. This effect may occur the shorter Au-CN and longer CN-Fe whencompared with the Ag derivative.[11b,11c,11d] In this work, however, only the shorter Au-CN can be observed with respect to the Ag-CN, which is the same as the previously reported case.[17] On the other hand, compounds**1** and **2**show a dramatic change of colour from yellow to red (HS to LS) during the change of spin states. This thermochromic phenomenon can be ascribed to the fact that the intensity of the metal-to-ligand charge transfer (MLCT) band around 550 nm increases, which is associated with the electron delocalization from the t_{2g} orbitals of the iron(II) to the π* orbitals of the ligands and enhanced by the spin state changes from HS to LS.[11c,15]

Considering the two-step spin transition of compounds**1** and **2**, we serve the former as an example for investigation. The crystallographic data of 225 K (the temperature of inflexion point between two steps) are collected. It is a pity that only one type of iron centre is observed as that at 300 K (HS) and 150 K (LS). We may infer that, on the one hand, two transient, slightly distinct iron(II) sites are generated absolutely during the change of spin state, but the limitation of crystallographic measurements and crystal resolutionmake it impossible to distinguish different iron(II) sites.[18] Then we are served an average view between HS and LS states, since the different sites situate in the structure in order. On the other hand, we also can't exclude the possibility of a disordered state in the inflexion point between two steps. The disordered intermediate state consists of a mix of HS and LS species at random in a long-range scale.[19]

For compound **3**, in contrast to previously reported highly symmetric 3D Hoffman-type structures,[9] its framework is pronouncedly distorted: the 2D $[FeNi(CN)_4]$ layers are notably corrugated due to the angle Fe-N3-C9 of 138.3(3)° and Fe-N4-C10 of 160.3(3)° deviating much from linearity; two adjacent pillared ligands are distorted in two configurations. These prominent distortions may influence the ligand field strength. We may also infer that the distortion of the framework makes it existing little void space to deposit guest molecules, which leads to the absence of supramolecular interactions. Then the iron centre in compound **3** prefers HS state with respect to most of symmetric SCO Hoffman-type systems. As a result, it exhibits characteristic paramagnetic behaviour in the temperature range investigated.

Conclusions

In this work, we have reported the synthesis, crystal structure, and magnetic propertiesof a series of cyanide-bridged bimetallic coordination polymers. Compounds **1** and **2** are isostructural to each otherand display complete two-step spin transition properties while **3** is characteristic of the HS state. The present work enriches the structural and magnetic properties of Hoffman-like systems. It can be foreseen that these materials provide potential applications of optical sensors by virtue of their thermochromic properties and switchable, multi-property materials.

This work was supported by the "973 Project" (2012CB821704), the NSFC (Grant nos 91122032, 21201182, 21373279 and 21121061) and Program for Changjiang Scholars and Innovative Research Team in University of China (IRT1298).

Notes and references

Key Laboratory of Bioinorganic and Synthetic Chemistry of Ministry of Education,
State Key Laboratory of Optoelectronic Materials and Technologies,
School of Chemistry and Chemical Engineering, Sun Yat-Sen University, Guangzhou 510275, P. R. China
Fax: (+86)20-8411-2245; Tel: (+86)20-8411-0966;
E-mail: tongml@mail.sysu.edu.cn.

† Electronic Supplementary Information (ESI) available: Selected bond lengths and angles for compounds **1**, **2** and **3**; supplementary structural figures for **1**; TG curve for**1** and **2**; Plot of $\chi_M T$ versus T for **3**. See DOI:10.1039/b000000x/

1 *Spin-Crossover Materials: Properties and Applications*; K. S. Murray, Ed.; Wiley-VCH: Weinheim, 2013.
2 J.-F. Létard, P.Guionneau and L. Goux-Capes, *Top. Curr. Chem.*, 2004, **235**, 221.
3 P. Gütlich and H. A. Goodwin, *Top. Curr.Chem.*, 2004, **233**, vol. 1-3.
4 P. Gütlich, A. Hauser and H. Spiering, *Angew. Chem. Int. Ed. Engl.*, 1994, **33**, 2024.
5 O. Kahn and C. J. Martinez, *Science*, 1998, **279**, 44.
6 (a) S. M. Neville, G. J. Halder, K. W.Chapman, M. B. Duriska, B. Moubaraki, K. S. Murray and C. J. Kepert, *J. Am. Chem. Soc.*, 2009,

131, 12106; (b) W.-T.; Liu, J.-Y.; Li, Z.-P.; Ni, X.; Bao, J.-L.; Liu, Y.-C.; Ou, J.-D.; Leng and M.-L. Tong, *Cryst. Growth Des.*, 2012, **12**, 1482; (c) W. Liu, X. Bao, L.-L. Mao, J. Tucek, R. Zboril, J.-L. Liu, F.-S. Guo, Z.-P. Ni and M.-L. Tong, *Chem. Commun.*, 2014, **50**, DOI: 10.1039/C3CC48935C.

7 (a) T. D. Roberts, F. Tuna, T. L. Malkin, C. A. Kilner and M. A. Halcrow, *Chem. Sci.*, 2012, **3**, 349; (b) X. Bao, J.-L. Liu, J.-D. Leng, Z. Lin, M.-L. Tong, M. Nihei and H. Oshio, *Chem. Eur. J.,* 2010, **16**, 7973; (c) X. Bao, P.-H. Guo, J.-L. Liu, J.-D. Leng and M.-L. Tong, *Chem. Eur. J.,* 2011, **17**, 2335; (d) X. Bao, P.-H. Guo, W. Liu, J. Tucek, W.-X. Zhang, J.-D. Leng, X.-M. Chen, I. Gural'skiy, L. Salmon, A. Bousseksou and M.-L. Tong, *Chem. Sci*., 2012, **3**, 1629; (e) Z. Yan, Z.-P. Ni, F.-S. Guo, J.-Y. Li, J.-L. Liu, W.-Q. Lin, D. Aravena, E. Ruiz and M.-L. Tong, *Inorg. Chem.*, 2014, **53**, 201.

8 J. Tao, R.-J. Wei, R.-B. Huang and L.-S. Zheng, *Chem. Soc. Rev*., 2012, **41**, 703.

9 M. C. Muñoz and J. A. Real, *Coord. Chem. Rev.,* 2011, **255**, 2068.

10 See for example: (a) G. Molnár, S. Cobo, J. A. Real, F. Carcenac, E. Daran, C. Vieu and A. Bousseksou, *Adv. Mater*., 2007, **19**, 2163; (b) G. Agustí, S. Cobo, A. B. Gaspar, G. Molnár, N. O. Moussa,P. Á. Szilágyi, V. Pálfi, C. Vieu, M. C.Muñoz, J. A. Real and A. Bousseksou, *Chem. Mater*., 2008, **20**, 6721; (c) P. D. Southon, L. Liu, E. A. Fellows, D. J. Price, G. J. Halder, K. W. Chapman, B. Moubaraki, K. S. Murray, J.-F. Létard and C. J. Kepert, *J. Am. Chem. Soc*., 2009, **131**, 10998; (d) M. Ohba, K. Yoneda, G. Agustí, M. C. Muñoz, A. B. Gaspar, J. A. Real, M. Yamasaki, H. Ando, Y. Nakao, S. Sakaki and S. Kitagawa, *Angew. Chem. Int. Ed.*, 2009, **48**, 4767; (e) R. Ohtani, K. Yoneda, S. Furukawa, N. Horike, S. Kitagawa, A. B. Gaspar, M. C. Muñoz, J. A.Real and M. Ohba, *J. Am. Chem. Soc*., 2011, **133**, 8600; (f) C. Bartual-Murgui, N. A. Ortega-Villar, H. J. Shepherd, M. C. Muñoz, L. Salmon, G. Molnár, A. Bousseksou and J. A. Real, *J. Mater. Chem*., 2011, **21**, 7217; (g) F. J.Muñoz-Lara, A. B. Gaspar, D. Aravena, E. Ruiz, M. C. Muñoz, M. Ohba, R. Ohtani, S. Kitagawa and J. A. Real, *Chem. Commun*., 2012, **48**, 4686; (h) N. F. Sciortino, K. R. Scherl-Gruenwald, G. Chastanet, G. J. Halder, K. W. Chapman, J.-F. Létard and C. J. Kepert, *Angew. Chem. Int. Ed*., 2012, **51**, 10154; (i) F. J. Muñoz-Lara, A. B. Gaspar, M. C. Muñoz, M. Arai, S. Kitagawa, M. Ohba and J. A. Real, *Chem. Eur. J*., 2012, **18**, 8013; (j) C. Bartual-Murgui, L. Salmon, A. Akou, N. A. Ortega-Villar, H. J. Shepherd, M. C. Muñoz, G. Molnár, J. A. Real and A. Bousseksou, *Chem. Eur. J*., 2012, **18**, 507; (k) X. Bao, H. J. Shepherd, L. Salmon, G. Molnár, M.-L. Tong and A. Bousseksou, *Angew. Chem. Int. Ed.*, 2013, **52**, 1198.

11 See for example: (a) V. Niel, M. C. Muñoz, A. B. Gaspar, A. Galet, G. Levchenko and J. A. Real, *Chem. Eur. J.*, 2002, **8**, 2446; (b) A. Galet, V. Niel, M. C.Muñoz and J. A. Real, *J. Am. Chem. Soc*., 2003, **125**, 14224; (c) V. Niel, A. L.Thompson, M. C. Muñoz, A. Galet, A. E. Goeta and J. A. Real, *Angew. Chem. Int . Ed*., 2003, **42**, 3760; (d) A. Galet, M. C. Muñoz, V. Martínez and J. A. Real, *Chem. Commun*., 2004, 2268; (e) A. Galet, M. C. Muñoz, A. B. Gaspar and J. A. Real, *Inorg. Chem*., 2005, **44**, 8749; (f) A. Galet, M. C. Muñoz and J. A. Real, *Chem. Commun.*, 2006, 4321; (g) M. C. Muñoz, A. B. Gaspar, A. Galet and J. A. Real, *Inorg. Chem.*, 2007, **46**, 8182. (h) T. Kosone, I. Tomori, C. Kanadani, T. Saito, T. Mochida and T. Kitazawa, *Dalton Trans*., 2010, **39**, 1719. (i) Z. Arcís-Castillo, M. C.Muñoz, G. Molnár, A. Bousseksou and J. A. Real, *Chem. Eur. J*., 2013, **19**, 6851.

12 D. Pocic, J.-M. Planeix, N. Kyritsakas, A. Jouaiti and M. W. Hosseini, *CrystEngComm*, 2005, **7**, 624.

13 G. M. Sheldrick, *SHELXTL97, program for crystal structure refinement*, University of Göttingen, Germany, 1997.

14 A. L. Spek, *Acta Cryst.* 2009, **D65**, 148.

15 G. Agustí, A. B. Gaspar, M. C. Muñoz and J. A. Real, *Inorg. Chem*., 2007, **46**, 9646.

16 M. Jansen, *Angew. Chem., Int. Ed. Engl*., 1987, **26**, 1098.

17 G. Agustí, M. C. Muñoz, A. B. Gaspar and J. A. Real, *Inorg. Chem*., 2008, **47**, 2552.

18 N. O. Moussa, E. Trzop, S. Zein, G. Molnár, E. Collet, A. B. Gaspar, J. A. Real, S. Borshch, K. Tanaka, H. Cailleau and A. Bousseksou, *Phys. Rev. B*, 2007, **75**, 054101.

19 J. A. Rodríguez-Velamazán, M. Castro, E. Palacios, R. Burriel, T. Kitazawa and T. Kawasaki, *J. Phys. Chem. B*, 2007, **111**, 1256.

TOC

Two isostructural cyanide-bridged bimetallic coordination polymers with 3D doubly interpenetrated Hoffman-like network exhibit complete two-step spin-crossover behaviours.